Hindawi
Journal of Nanomaterials
Volume 2018, Article ID 5167182, 7 pages
https://doi.org/10.1155/2018/5167182

Research Article

An Eco-Friendly Method of $BaTiO_3$ Nanoparticle Synthesis Using Coconut Water

Maria de Andrade Gomes,[1] **Lucas Gonçalves Magalhães**,[1,2] **Alexandre Rocha Paschoal**,[3] **Zélia Soares Macedo**,[4] **Álvaro Silva Lima**,[1,2] **Katlin Ivon Barrios Eguiluz**,[1,2] **and Giancarlo Richard Salazar-Banda**[1,2]

[1]*Instituto de Tecnologia e Pesquisa, Universidade Tiradentes, 49032-490 Aracaju, SE, Brazil*
[2]*Programa de Pós Graduação em Engenharia de Processos, Universidade Tiradentes, 49032-490 Aracaju, SE, Brazil*
[3]*Laboratório de Espectroscopia Vibracional e Microscopia, Departamento de Física, Universidade Federal do Ceará, 60455-760 Fortaleza, CE, Brazil*
[4]*Laboratório de Preparação e Caracterização de Materiais, Departamento de Física, Universidade Federal de Sergipe, 49000-100 São Cristóvão, SE, Brazil*

Correspondence should be addressed to Maria de Andrade Gomes; maria.fisica@gmail.com

Received 3 April 2018; Revised 8 June 2018; Accepted 1 July 2018; Published 17 July 2018

Academic Editor: Victor M. Castaño

$BaTiO_3$ nanoparticles were successfully synthesized by a new coconut water-based sol–gel method using $Ba(CH_3COO)_2$ and $TiCl_3$ as the starting salts. The influence of the amount of coconut water and calcination conditions on the barium titanate crystallization was investigated. The resulting nanoparticles were characterized by thermogravimetric and differential thermal analysis, X-ray diffraction, scanning electron microscopy, and Raman and Fourier transform infrared (FTIR) spectroscopies. The ferroelectric tetragonal single phase of $BaTiO_3$ was obtained in samples prepared with a ratio of coconut water volume (mL)/$BaTiO_3$ mass (g) of 25 : 2 and 30 : 2, calcined at 1100°C, which was confirmed by XRD measurements. Crystallites with an average size of about 31 nm for both samples were obtained, and microscopy images revealed the presence of particles in the range of 40 to 60 nm. Raman and FTIR spectra confirmed the dominant tetragonal phase of $BaTiO_3$, meanwhile traces of $BaCO_3$ were identified in FTIR spectra.

1. Introduction

Barium titanate ($BaTiO_3$—BT) is a well-known ferroelectric material widely used in the manufacture of multilayer ceramic capacitors (MLCCs) [1], thermistors [2], and electrooptic devices [3]. $BaTiO_3$ also exhibits piezoelectric, pyroelectric, and catalytic properties, suitable for sonar and infrared detectors [4], oxidation catalysts [5], and photocatalysts [6].

The recent demand for miniaturization of electronic devices requires the dielectric layer thickness to be reduced to a few hundred nanometers. As a consequence, the particle size of the $BaTiO_3$ raw material needs to be less than a few hundred nanometers. To achieve this, an adequate synthesis procedure needs to be employed.

Barium titanate is traditionally prepared by the solid-state mixing of $BaCO_3$ and TiO_2. High calcination temperatures and intense ball-milling are required in this procedure to promote slow solid-state diffusion [7]. As an alternative, different wet chemical methods have been employed to produce $BaTiO_3$ nanometer-scale powders including sol–gel, Pechini, sol–emulsion–gel, and solvothermal and coprecipitation methods. These methods allow precursor homogeneity at an atomic level and employ lower calcination temperatures compared with a conventional solid-state method [8]. The main problems in using these wet chemical

procedures are the highly toxic and hazardous precursors and solvents, the long duration of the reaction process, and the possibility of contamination by modifying agents (mineralizing and precipitation agents) [8, 9].

At the same time, other innovative routes proposed in the literature for $BaTiO_3$ synthesis frequently use toxic precursors (organometallics) and have multistep reactions. For example, Han and coworkers obtained $BaTiO_3$ in the cubic phase at low temperature using a new LSS (liquid–solid–solution) approach, which involved the preparation of a heterogeneous mixture with three immiscible layers followed by refluxing at 80°C for 2 h. The $BaTiO_3$ nanoparticles were produced in the presence of sodium hydroxide as a catalyst and oleic acid as a capping agent, using an organometallic compound as a Ti source and n-butanol as a solvent [10].

In this way, we have developed a green methodology to synthesize barium titanate nanoparticles via a coconut water-based sol–gel route. This modified sol–gel route is straightforward and has proven to be effective in the synthesis of nanoparticles and thin films [11–14]. Due to the high complexity of the coconut water composition, the exact mechanism of sol–gel stabilization and particle formation is still unknown. Some reports state that the large protein chains present in the coconut water can easily bind the metal salts of the solution to form stable micelles [15, 16]. Successful synthesis of gold nanoparticles assisted by a protein mixture [17] and metal oxide nanocrystals using collagen have been recently reported [18], supporting the efficiency of proteins in the production of crystalline nanoparticles. Indeed, metal ions can bind to specific amino acid (aa) ligands of the protein chain depending on the characteristics of the metal ion (e.g., valence state and ionic radius) and the protein chain (e.g., net charge, dipole moment, and polarizability, among others) [19]. On the other hand, sugars may also play a role in this process, since they are the main solute constituents of coconut water [20]. Sucrose and glucose—the more abundant sugars in coconut water—have been used to produce different metal and metal oxide nanoparticles by acting as both chelating agents and fuel during calcination [21–23].

The developed method has important advantages over conventional methods, including low toxicity, simplicity of processing, and exemption of the need for organic solvents and sophisticated equipment. Its environmentally friendly character is derived from the fact that it uses nitrates, carbonates, and chlorides instead of organometallic compounds as metal sources and employs coconut water as a natural polymerization agent. Additionally, the coconut itself can be completely consumed along its supply chain, reducing the production of waste. For example, coconut oil (extracted from the dried flesh) and coconut husk and shell have shown great potential in clean energy production, such as biodiesel [24] and biomass fuel [25].

In this study, the influence of the calcination temperature and the amount of coconut water on the crystallization of the $BaTiO_3$ perovskite phase were evaluated. The produced nanoparticles were characterized by means of simultaneous differential thermal analysis (DTA) and thermogravimetry (TG), X-ray diffraction (XRD), field emission gun scanning electron microscopy (FEG-SEM), Fourier transform infrared spectroscopy (FTIR), and Raman spectroscopy.

2. Experimental

For $BaTiO_3$ powder synthesis via the alternative sol–gel route proposed, $Ba(CH_3COO)_2$ and $TiCl_3$ (15% solution in HCl) were used as starting materials. Initially, stoichiometric amounts of $Ba(CH_3COO)_2$ were dissolved in distilled water. The volume of water was fixed at 5 mL/g of $BaTiO_3$ produced, which was enough to completely dissolve the salt. Subsequently, 3.34 mL of $TiCl_3$ acid solution was added to the Ba solution under magnetic stirring. Filtered coconut water was then added to the mixture, followed by stirring for 30 min. Different samples were produced according to the volume/mass ratio (mL/g) of coconut water (CW) and $BaTiO_3$ (BT) powder produced as follows: CW : BT = 5 : 2, 10 : 2, 15 : 2, 20 : 2, 25 : 2, and 30 : 2. The final solutions were dried at 200°C overnight with continuous magnetic stirring and then preheated at 400°C for 5 h. Finally, the obtained xerogels were calcined at 1000 or 1100°C for 4 h.

DTA/TG measurements of the preheated samples were performed in a simultaneous DTA/TG system (NETZSCH STA 449 F1 Jupiter) at a heating rate of 10°C/min in N_2 flow. The powders' crystalline structure was investigated by XRD using Co Kα radiation (Rigaku RINT 2000/PC), in a 2θ range from 20° to 80°, with a scan speed of 1°/min in continuous mode. The size of the crystallites was estimated from the full width at half maximum (FWHM) of diffraction peaks using the Scherrer equation. Particle size and morphology were determined from scanning electron microscopy (JEOL JSM-6510LV) images. Raman spectra were recorded in a WITec alpha300 equipped with a Nd:YAG laser (2.33 eV, 532 nm) and a Nikon lens (20x; NA = 0.40). The scattered light was detected with a spectrometer equipped with a diffraction grating at 1800 I/mm and a charge-coupled device (CCD). For each spectrum, three accumulations of 30 s were performed, with an incident power on the sample surface of 630 μW. The FTIR spectra were acquired using Bruker VERTEX 70v equipment with a Platinum ATR accessory and evacuated chamber. A total of 128 scans with a resolution of 2 cm^{-1} were acquired.

3. Results and Discussion

Figure 1 presents the DTA/TG data for a sample preheated at 400°C. The curves can be divided into three stages. The first stage is characterized by endothermic peaks and 15% of mass loss, which are associated with desorption of gas and water molecules from particle surfaces [26, 27]. In the second stage, a large exothermic peak between 400 and 900°C with a very low loss of mass is observed, which can be related to the formation of intermediate phases and solid-phase transition in the sample [28]. The temperature range of 200 to 600°C is a typical region of organic degradation, and the low loss of mass observed in this region indicates a low content of remainder organic matter in the preheated sample. The exothermic peak in the third

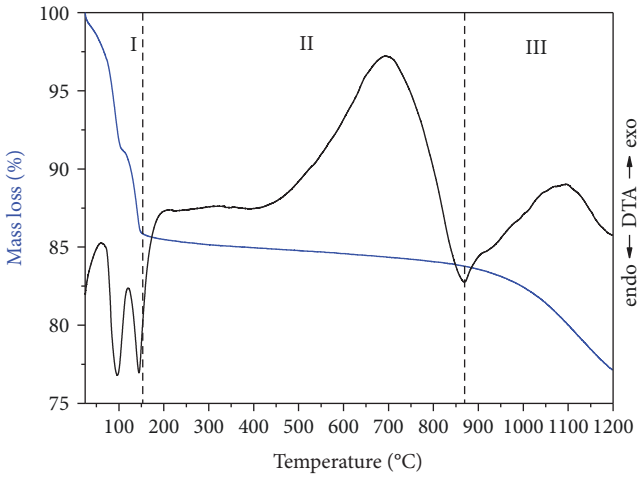

Figure 1: DTA/TG curves of powder preheated at 400°C.

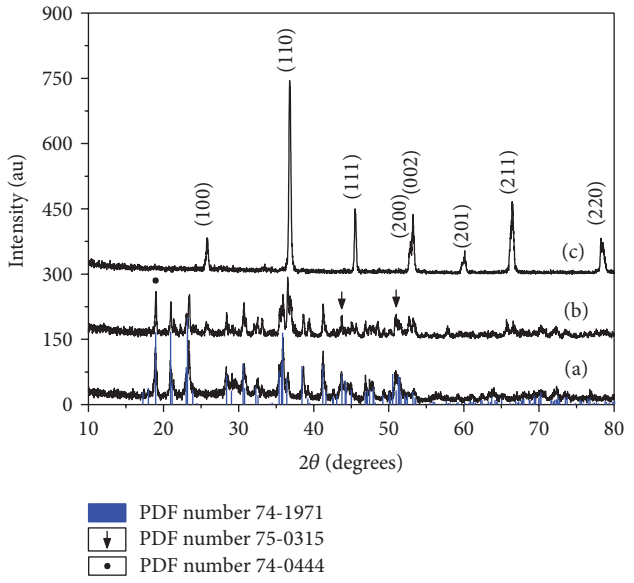

Figure 2: X-ray diffraction patterns for samples prepared with a CW/BT ratio of 25 : 2 calcined at (a) 400°C, (b) 1000°C, and (c) 1100°C.

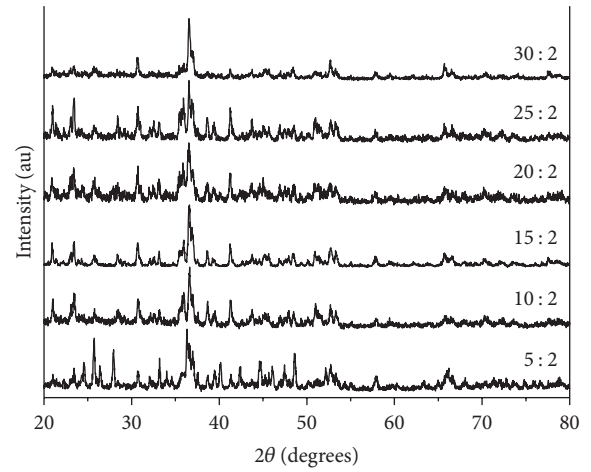

Figure 3: XRD patterns of different samples with differing CW : BT ratios (identified in the figure) calcined at 1000°C for 4 h.

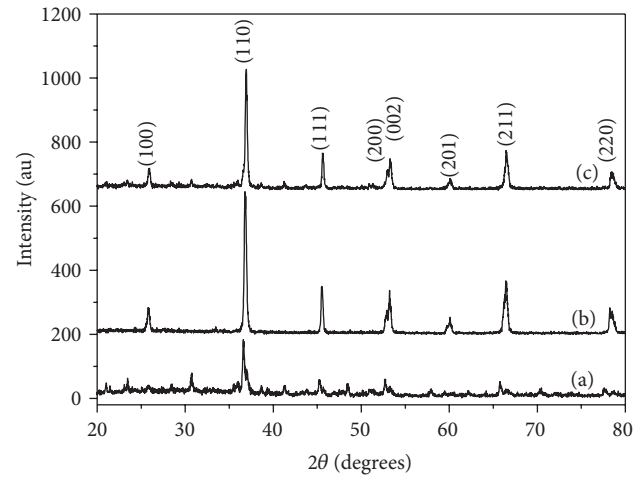

Figure 4: XRD patterns of samples prepared with a CW : BT ratio of (a) 20 : 2, (b) 25 : 2, and (c) 30 : 2 calcined at 1100°C for 4 h.

stage at around 1100°C corresponds to $BaTiO_3$ crystallization, followed by a mass loss of about 7% due to release of HCl, O_2, and H_2 species. At the end of the reaction, the total weight loss was about 23%.

Figure 2 presents the diffraction patterns for samples prepared with a CW : BT ratio of 25 : 2 thermally treated at (a) 400°C, (b) 1000°C, and (c) 1100°C. For the sample annealed at 400°C (pattern (a)), a mixture of intermediate Ba and Ti phases, such as titanium oxide (PDF number 75-0315), titanium chloride (PDF number 74-0444), and barium chloride (PDF number 74-1971), could be detected. Nonidentified peaks are also present. This mixture of intermediate phases is maintained in the sample treated at 1000°C, with small differences in the peak intensity ratios as can be observed in pattern (b), which corroborates the thermal events that occurred in the second stage of the DTA/TG curves (Figure 1). In pattern (c), the perovskite phase of $BaTiO_3$ (PDF number 79-2265) was obtained after calcination at 1100°C for 4 h in accordance with the DTA/TG results (third stage of Figure 1).

To study the influence of the amount of coconut water (CW : BT ratios) and calcination conditions on the crystallization of the $BaTiO_3$ phase, diffractograms of the powders synthesized with different CW : BT ratios and calcined at 1000°C for 4 h were examined (see Figure 3). Intermediate phases are present in all samples, demonstrating that the thermal treatment employed (1000°C) was insufficient to obtain single-phase $BaTiO_3$ in all samples.

A different behavior was observed for samples calcined at 1100°C. The diffractograms are presented in Figure 4. For the sample prepared with a CW : BT ratio of 20 : 2 (pattern (a)), the $BaTiO_3$ main peaks are of low intensity and appear with various unidentified peaks. The samples that were prepared with a CW : BT ratio of 25 : 2 (pattern (b)) and 30 : 2 (pattern (c)) show that the perovskite

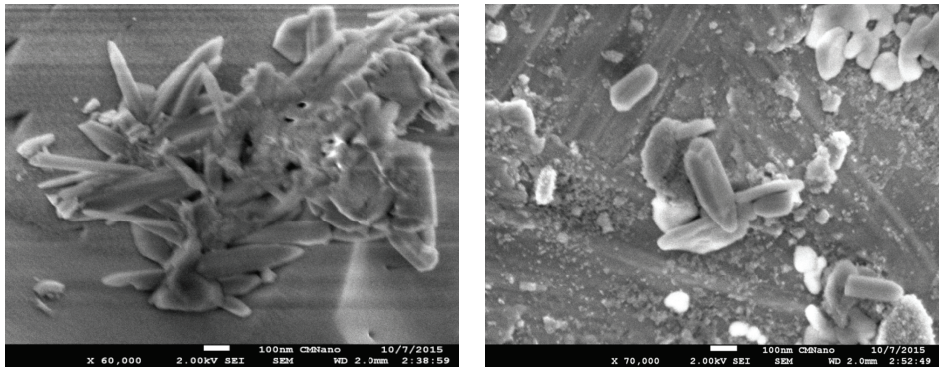

(a) (b)

Figure 5: FEG-SEM images of a sample prepared with a CW : BT ratio of 25 : 2 treated at 1100°C for 4 h.

$BaTiO_3$ phase was achieved. In both diffraction patterns, an asymmetrical peak at $2\theta \approx 53^\circ$ is clearly observed. The splitting or asymmetry of reflection in this region is a result of distortion in the unit cell, characteristic of tetragonal phase $BaTiO_3$.

The crystallite size of these two samples was estimated by a broadening of the diffraction peaks using the Scherrer equation, which is given by

$$D = \frac{K.\lambda}{B.\cos\theta_B}. \quad (1)$$

In this equation, $K = 0.89$ is the Scherrer constant, λ is the wavelength of X-rays ($\lambda = 1.788965$ Å for Co Kα radiation), θ_B is the peak position, and B is the full width at half maximum (FWHM) of the peak. The crystallite size determined for both samples was averaged at 31 nm.

Some authors had previously produced pure and doped barium titanate using the conventional sol–gel method. Hao et al. [29] used the standard sol–gel procedure to prepare pure and Ag, La-codoped $BaTiO_3$ samples calcined at 1100°C, similar to the temperature used in the present study. The powders were crystallized in the (paraelectric) cubic structure of barium titanate, and considerable amounts of barium carbonate (a common by-product of barium titanate production) were detected by XRD. Cernea et al. [30] produced Ce-doped $BaTiO_3$ also at 1100°C. The sample presented a diffraction pattern consistent with the cubic phase (no peak splitting of the tetragonal phase could be detected) and various nonidentified peaks of low intensity. The cubic $BaTiO_3$ phase has also been obtained at lower calcination temperatures using a conventional sol–gel procedure [31, 32].

Some drawbacks arising from the conventional sol–gel methodology can be seen in all of the above-mentioned studies: they use highly toxic alkoxide precursors and organic solvents as well as multistep procedures involving pH adjustment and reflux and require highly controlled hydrolysis and polycondensation reactions. On the other hand, the modified sol–gel method with coconut water is a one-step procedure that uses metallic salts as the chemical precursor, distilled water as the solvent, and coconut water as the polymerization agent of the departure solution. No toxic organic solvents, surfactants, and chelating or intermediate precursors are necessary, which highlights the low toxicity and eco-friendly character of the proposed alternative sol–gel methodology for large-scale production.

Figure 5 displays FEG-SEM images of a sample prepared with a CW : BT ratio of 25 : 2 annealed at 1100°C for 4 h taken from different regions of the powder dispersion. A predominant rod-like morphology can be observed in both regions with structures that are 200–400 nm in length. The nonequiaxial growth of $BaTiO_3$ particles with a tetragonal crystalline structure has also been recently reported using $BaTiO_3$ powders produced by a hydrothermal method [33], sonochemical synthesis followed by thermal treatment [34], and a solvothermal method using ethylene glycol as a solvent [35]. Rod-shaped particles are particularly advantageous in catalysis applications. The surface-to-volume ratio is higher in nanorods and nanowires compared to nanospheres, which guarantees a higher density of active sites exposed for surface catalytic reactions [36].

The tetragonal polymorph of perovskite $BaTiO_3$ is ferroelectric—it retains spontaneous polarization, which is reversible under an applied electric field [37]. Unlike the cubic structure of $BaTiO_3$, the tetragonal structure is capable of storing a large amount of potential energy due to the distortion of the Ti^{4+} ions from a centrosymmetric to an asymmetric position within the TiO_6 octahedron (as illustrated in Figure 6), resulting in high values of dielectric constant [38]. It is the ferroelectric character of the material that is responsible for the various practical applications of barium titanate ceramics.

Although the identification of crystalline structures by XRD measurements was carried out (probing the global structure of the sample), Raman spectroscopy was also employed as it is a highly sensitive technique, more suited to probing the local structure of a material on an atomic scale based on vibrational symmetry. Figure 7 presents the Raman spectra for 25 : 2 and 30 : 2 (CW : BT ratio) samples, both calcined at 1100°C. Both samples showed similar spectra consistent with those reported in the literature for $BaTiO_3$ crystals produced by a solid-state method [39]. The dominant tetragonal phase is confirmed by the presence of a sharp and distinct peak at 303 cm^{-1} assigned to E(TO) mode, which indicates asymmetry within the TiO_6 octahedron of $BaTiO_3$

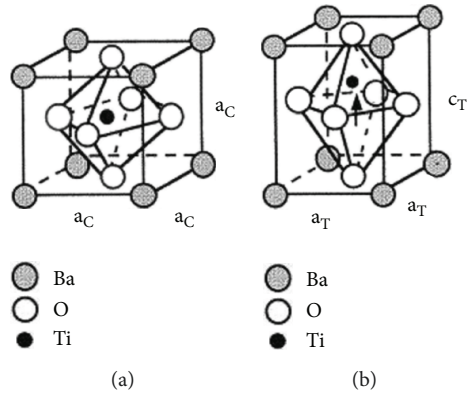

FIGURE 6: Perovskite structure of $BaTiO_3$: (a) the cubic structure in the paraelectric phase; (b) the tetragonal structure in the ferroelectric phase (adapted from [37]).

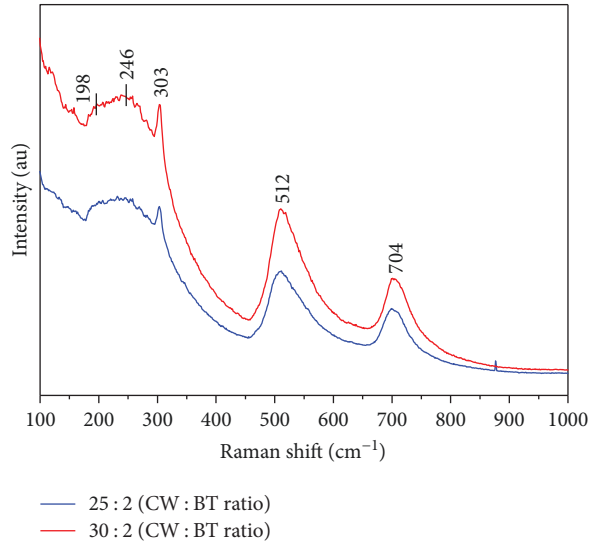

FIGURE 7: Raman spectra for samples prepared with CW : BT ratios of 25 : 2 and 30 : 2 and calcined at 1100°C for 4 h.

on a local scale [40]. The peaks at 198, 246, 512, and 704 cm^{-1} also indicate the formation of the tetragonal phase [41, 42]. Among these, the peaks at 303 and 703 cm^{-1} disappear above the Curie temperature, which is the stable region for the cubic phase [43]. This means that it is possible to discern between the cubic and tetragonal phases by the presence of these two peaks in the Raman spectrum. Finally, the asymmetry in the 515 cm^{-1} peak suggests the presence of coupling TO modes associated with the tetragonal phase [42]. Thus, the Raman experiments support the XRD measurements regarding the structural phases present in both samples.

The FTIR spectra of samples prepared using CW : BT ratios of 25 : 2 and 30 : 2 shown in Figure 8 provide complementary information to the Raman experiments. Both samples have a broad absorption band at 3000–3500 cm^{-1} (symmetric and asymmetric stretching vibrations of O–H) and double peaks at 1600 and 1632 cm^{-1} (symmetric stretching of carboxylate groups and bending vibration of H–O–H, resp.) with a higher intensity in the sample prepared with a

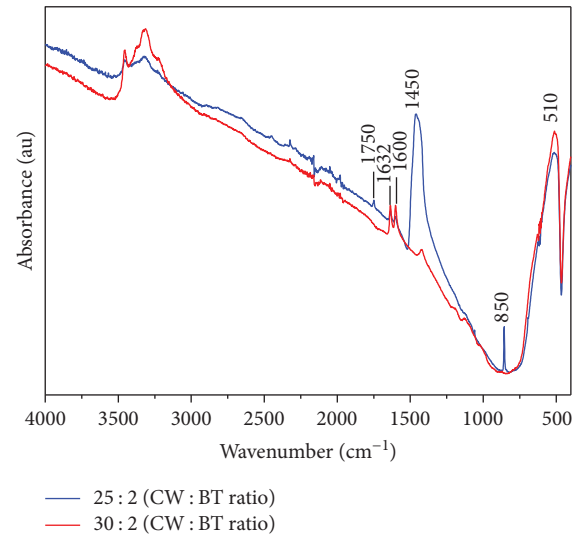

FIGURE 8: FTIR spectra for samples prepared using CW : BT ratios of 25 : 2 and 30 : 2 and calcined at 1100°C for 4 h.

30 : 2 CW : BT ratio [44]. The $BaTiO_3$ phase is confirmed by the peak at 510 cm^{-1}, which is related to Ti–O absorption in the barium titanate lattice [45]. A strong absorption at 1450 cm^{-1} can be observed for the sample prepared with a CW : BT ratio of 25 : 2, which—as well as the ones at 1750 and 850 cm^{-1}—is due to asymmetric stretching of the carbonate ions (CO_3^{2-}) of $BaCO_3$ [45]. $BaCO_3$ could not be detected by XRD in the 25 : 2 sample. Its presence, however, was evidenced by FTIR—a sensitive technique that can detect traces of impurities such as barium carbonate in very small quantities (~0.6 wt%) [46]. Theoretically, the origin of barium carbonate in $BaTiO_3$ samples produced by sol–gel methodologies is due to the reaction between hydrolyzed barium species and atmospheric CO_2 [47]. According to Arvanitidis and coworkers [48], barium carbonate is a stable compound whose decomposition is completed above 1600 K (~1327°C). Hence, its presence in the samples calcined at 1100°C is reasonable.

4. Conclusions

In this work, a green methodology for the preparation of $BaTiO_3$ nanoparticles is suggested. The proposed modified sol–gel method employs filtered coconut water as the polymerization agent of the precursor solution, and it proves to be highly efficient. The samples produced using CW : BT ratios of 25 : 2 and 30 : 2 and calcined at 1100°C for 4 h presented the single crystalline phase of $BaTiO_3$. In the XRD patterns, the tetragonal form of $BaTiO_3$, evidenced by the splitting of the (200)/(002) peak, was detected in both samples. The Raman spectra confirmed the presence of the dominant tetragonal phases. Traces of barium carbonate were detected in the 25 : 2 (CW : BT ratio) sample. The average crystallite size was estimated at 31 nm by the Scherrer equation, while electron micrographs showed samples composed of round particles with diameters of 40–60 nm and elongated structures of 200–400 nm in length. The results

demonstrate a potential application in the manufacture of electrooptic devices using the $BaTiO_3$ nanoparticles produced in this work.

Data Availability

The XRD, FTIR, and Raman data used to support the findings of this study are available from the corresponding author upon request.

Conflicts of Interest

There are no conflicts of interest to declare.

Acknowledgments

This work was supported by Conselho Nacional de Desenvolvimento Científico e Tecnológico (CNPq) (Grant nos. 310282/2013-6 and 304419/2015-0), Coordenação de Aperfeiçoamento de Pessoal de Nível Superior (CAPES), and Fundação de Apoio à Pesquisa e à Inovação Tecnológica do Estado de Sergipe (Fapitec/SE). The authors thank the CMNano-UFS microscopy center for microscopy facilities.

References

[1] P. Wang, H. Xu, G. Zhu, Y. Zhao, J. Li, and A. Yu, "An efficient method to achieve MLCC miniaturization and ensure its reliability," *Journal of Materials Science: Materials in Electronics*, vol. 28, no. 5, pp. 4102–4106, 2016.

[2] C. Gao, Q. Fu, D. Zhou et al., "Nanocrystalline semiconducting donor-doped $BaTiO_3$ ceramics for laminated PTC thermistor," *Journal of the European Ceramic Society*, vol. 37, no. 4, pp. 1523–1528, 2017.

[3] P. Castera, A. M. Gutierrez, D. Tulli et al., "Electro-optical modulation based on Pockels effect in BaTiO3 with a multidomain structure," *IEEE Photonics Technology Letters*, vol. 28, no. 9, pp. 990–993, 2016.

[4] B. Ertug, "The overview of the electrical properties of barium titanate," *American Journal of Engineering Research*, vol. 2, pp. 1–7, 2013.

[5] V. Albaladejo-Fuentes, F. López-Suárez, M. S. Sánchez-Adsuar, and M. J. Illán-Gómez, "$BaTi_{0.8}Cu_{0.2}O_3$ catalyst for NO oxidation and NO_x storage: effect of synthesis method," *Topics in Catalysis*, vol. 60, no. 3-5, pp. 220–224, 2017.

[6] M. Thamima, Y. Andou, and S. Karuppuchamy, "Microwave assisted synthesis of perovskite structured $BaTiO_3$ nanospheres via peroxo route for photocatalytic applications," *Ceramics International*, vol. 43, no. 1, pp. 556–563, 2017.

[7] M. Ganguly, S. K. Rout, C. W. Ahn, I. W. Kim, and M. Kar, "Structural, electrical and optical properties of $Ba(Ti_{1-x}Yb_{4x/3})O_3$ ceramics," *Ceramics International*, vol. 39, no. 8, pp. 9511–9524, 2013.

[8] M. A. Gomes, A. S. Lima, K. I. B. Eguiluz, and G. R. Salazar-Banda, "Wet chemical synthesis of rare earth-doped barium titanate nanoparticles," *Journal of Materials Science*, vol. 51, no. 10, pp. 4709–4727, 2016.

[9] G. Philippot, C. Elissalde, M. Maglione, and C. Aymonier, "Supercritical fluid technology: a reliable process for high quality $BaTiO_3$ based nanomaterials," *Advanced Powder Technology*, vol. 25, no. 5, pp. 1415–1429, 2014.

[10] W. Han, H.-S. Lee, B. Yoo, and H.-H. Park, "Evaluation of Na_2TiO_3 formation for producing crystalline $BaTiO_3$ nanoparticles by liquid-solid-solution process at low temperature," *Journal of Alloys and Compounds*, vol. 695, pp. 2160–2164, 2017.

[11] P. J. R. Montes, M. E. G. Valerio, M. A. Macêdo, F. Cunha, and J. M. Sasaki, "Yttria thin films doped with rare earth for applications in radiation detectors and thermoluminescent dosimeters," *Microelectronics Journal*, vol. 34, no. 5-8, pp. 557–559, 2003.

[12] P. C. A. Brito, R. F. Gomes, J. G. S. Duque, and M. A. Macêdo, "$SrFe_{12}O_{19}$ prepared by the proteic sol–gel process," *Physica B*, vol. 384, no. 1-2, pp. 91–93, 2006.

[13] M. de Andrade Gomes, M. E. G. Valerio, and Z. S. Macedo, "Particle size control of Y_2O_3:Eu^{3+} prepared via a coconut water assisted sol–gel method," *Journal of Nanomaterials*, vol. 2011, Article ID 469685, 6 pages, 2011.

[14] W. M. S. Silva, N. S. Ferreira, J. M. Soares, R. B. da Silva, and M. A. Macêdo, "Investigation of structural and magnetic properties of nanocrystalline Mn-doped $SrFe_{12}O_{19}$ prepared by proteic sol–gel process," *Journal of Magnetism and Magnetic Materials*, vol. 395, pp. 263–270, 2015.

[15] J. A. C. de Paiva, M. P. F. Graça, J. Monteiro, M. A. Macedo, and M. A. Valente, "Spectroscopy studies of $NiFe_2O_4$ nanosized powders obtained using coconut water," *Journal of Alloys and Compounds*, vol. 485, no. 1-2, pp. 637–641, 2009.

[16] E. P. Muniz, J. R. C. Proveti, R. D. Pereira et al., "Influence of heat-treatment environment on Ni-ferrite nanoparticle formation from coconut water precursor," *Journal of Materials Science*, vol. 48, no. 4, pp. 1543–1554, 2013.

[17] N. Goswami, R. Saha, and S. K. Pal, "Protein-assisted synthesis route of metal nanoparticles: exploration of key chemistry of the biomolecule," *Journal of Nanoparticle Research*, vol. 13, no. 10, pp. 5485–5495, 2011.

[18] T. P. Braga, D. F. Dias, M. F. de Sousa, J. M. Soares, and J. M. Sasaki, "Synthesis of air stable FeCo alloy nanocrystallite by proteic sol–gel method using a rotary oven," *Journal of Alloys and Compounds*, vol. 622, pp. 408–417, 2015.

[19] T. Dudev and C. Lim, "Competition among metal ions for protein binding sites: determinants of metal ion selectivity in proteins," *Chemical Reviews*, vol. 114, no. 1, pp. 538–556, 2013.

[20] J. M. de Carvalho, G. A. Maia, P. H. de Sousa, and G. A. Junior, "Water of coconut: nutritional and functional properties and processing," *Semina: Ciências Agrárias*, vol. 27, pp. 437–452, 2006.

[21] O. V. Kharissova, H. V. Rasika Dias, B. I. Kharisov, B. O. Pérez, and V. M. Jiménez Pérez, "The greener synthesis of nanoparticles," *Trends in Biotechnology*, vol. 31, no. 4, pp. 240–248, 2013.

[22] L. Xu, B. Wei, Z. Zhang, Z. Lü, H. Gao, and Y. Zhang, "Synthesis and luminescence of europium doped yttria nanophosphors via a sucrose-templated combustion method," *Nanotechnology*, vol. 17, no. 17, pp. 4327–4331, 2006.

[23] Z. Wang, G. M. Kale, and M. Ghadiri, "Sol–gel production of $Ce_{0.8}Gd_{0.2}O_{1.9}$ nanopowders using sucrose and pectin as organic precursors," *Journal of the American Ceramic Society*, vol. 95, no. 9, pp. 2863–2868, 2012.

[24] T. Qiu, X. Guo, J. Yang et al., "The synthesis of biodiesel from coconut oil using novel Brønsted acidic ionic liquid as green catalyst," *Chemical Engineering Journal*, vol. 296, pp. 71–78, 2016.

[25] I. Ali, H. Bahaitham, and R. Naebulharam, "A comprehensive kinetics study of coconut shell waste pyrolysis," *Bioresource Technology*, vol. 235, pp. 1–11, 2017.

[26] D. Neuhaus, "Water adsorption and desorption pretreatment of surfaces increases the maximum amount of adsorbed water molecules by a multiple," *Adsorption*, vol. 19, no. 6, pp. 1127–1135, 2013.

[27] K. Goren, L. Chen, L. S. Schadler, and R. Ozisik, "Influence of nanoparticle surface chemistry and size on supercritical carbon dioxide processed nanocomposite foam morphology," *The Journal of Supercritical Fluids*, vol. 51, no. 3, pp. 420–427, 2010.

[28] P. Durán, F. Capel, J. Tartaj, D. Gutierrez, and C. Moure, "Heating-rate effect on the $BaTiO_3$ formation by thermal decomposition of metal citrate polymeric precursors," *Solid State Ionics*, vol. 141-142, pp. 529–539, 2001.

[29] S. Hao, J. Li, W. Wang, D. Fu, C. Wang, and Q. Shang, "Effects of Ag-La codoping on structural and electrical properties of $BaTiO_3$ powder," *Research on Chemical Intermediates*, vol. 39, no. 6, pp. 2705–2713, 2013.

[30] M. Cernea, O. Monnereau, P. Llewellyn, L. Tortet, and C. Galassi, "Sol–gel synthesis and characterization of Ce doped-$BaTiO_3$," *Journal of the European Ceramic Society*, vol. 26, no. 15, pp. 3241–3246, 2006.

[31] M. Cernea, C. E. Secu, B. S. Vasile, and M. Secu, "Structural and optical characterization of sol–gel derived Tm-doped $BaTiO_3$ nanopowders and ceramics," *Current Applied Physics*, vol. 13, no. 1, pp. 137–141, 2013.

[32] A. C. Ianculescu, C. A. Vasilescu, M. Crisan et al., "Formation mechanism and characteristic of lanthanum-doped $BaTiO_3$ powders and ceramics prepared by the sol–gel process," *Materials Characterization*, vol. 106, pp. 195–207, 2015.

[33] K. C. Verma, V. Gupta, J. Kaur, and R. K. Kotnala, "Raman spectra, photoluminescence, magnetism and magnetoelectric coupling in pure and Fe doped $BaTiO_3$ nanostructures," *Journal of Alloys and Compounds*, vol. 578, pp. 5–11, 2013.

[34] D. P. Dutta, A. Ballal, J. Nuwad, and A. K. Tyagi, "Optical properties of sonochemically synthesized rare earth ions doped $BaTiO_3$ nanophosphors: probable candidate for white light emission," *Journal of Luminescence*, vol. 148, pp. 230–237, 2014.

[35] M. Inada, N. Enomoto, K. Hayashi, J. Hojo, and S. Komarneni, "Facile synthesis of nanorods of tetragonal barium titanate using ethylene glycol," *Ceramics International*, vol. 41, no. 4, pp. 5581–5587, 2015.

[36] B. Wang, D. Xue, and Y. Shi, *Nanorods, Nanotubes, and Nanomaterials Research Progress*, W. V. Prescott and A. I. Schwartz, Eds., Nova Science Publisher, New York, 2008.

[37] L. B. Kong, T. S. Zhang, J. Ma, and F. Boey, "Progress in synthesis of ferroelectric ceramic materials via high-energy mechanochemical technique," *Progress in Materials Science*, vol. 53, no. 2, pp. 207–322, 2008.

[38] N. Nuraje and K. Su, "Perovskite ferroelectric nanomaterials," *Nanoscale*, vol. 5, no. 19, pp. 8752–8780, 2013.

[39] H. Hayashi, T. Nakamura, and T. Ebina, "In-situ Raman spectroscopy of $BaTiO_3$ particles for tetragonal–cubic transformation," *Journal of Physics and Chemistry of Solids*, vol. 74, no. 7, pp. 957–962, 2013.

[40] P. S. Dobal, A. Dixit, and R. S. Katiyar, "Effect of lanthanum substitution on the Raman spectra of barium titanate thin films," *Journal of Raman Specroscopy*, vol. 38, no. 2, pp. 142–146, 2007.

[41] Z. Ž. Lazarević, M. M. Vijatović, B. D. Stojanović, M. J. Romčević, and N. Ž. Romčević, "Structure study of nanosized La- and Sb-doped $BaTiO_3$," *Journal of Alloys and Compounds*, vol. 494, no. 1-2, pp. 472–475, 2010.

[42] U. A. Joshi, S. Yoon, S. Baik, and J. S. Lee, "Surfactant-free hydrothermal synthesis of highly tetragonal barium titanate nanowires: a structural investigation," *The Journal of Physical Chemistry. B*, vol. 110, no. 25, pp. 12249–12256, 2006.

[43] G. Yang, Z. Yue, T. Sun, J. Zhao, Z. Yang, and L. Li, "Investigation of ferroelectric phase transition for modified barium titanate in multilayer ceramic capacitors by in situ Raman scattering and dielectric measurement," *Applied Physics A: Materials Science & Processing*, vol. 91, no. 1, pp. 119–125, 2008.

[44] W. Wang, L. Cao, W. Liu, G. Su, and W. Zhang, "Low-temperature synthesis of $BaTiO_3$ powders by the sol–gel-hydrothermal method," *Ceramics International*, vol. 39, no. 6, pp. 7127–7134, 2013.

[45] A. G. A. Darwish, Y. Badr, M. El Shaarawy, N. M. H. Shash, and I. K. Battisha, "Influence of the Nd^{3+} ions content on the FTIR and the visible up-conversion luminescence properties of nano-structure $BaTiO_3$ prepared by sol–gel technique," *Journal of Alloys and Compounds*, vol. 489, no. 2, pp. 451–455, 2010.

[46] L. Ramajo, R. Parra, M. Reboredo, M. Zaghete, and M. Castro, "Heating rate and temperature effects on the $BaTiO_3$ formation by thermal decomposition of (Ba, Ti) organic precursors during the Pechini process," *Materials Chemistry and Physics*, vol. 107, no. 1, pp. 110–114, 2008.

[47] C. Lemoine, B. Gilbert, B. Michaux, J.-P. Pirard, and A. J. Lecloux, "Synthesis of barium titanate by the sol-gel process," *Journal of Non-Crystalline Solids*, vol. 175, no. 1, pp. 1–13, 1994.

[48] I. Arvanitidis, D. Siche, and S. Seetharaman, "A study of thermal decomposition of $BaCO_3$," *Metallurgical and Materials Transactions B: Process Metallurgy and Materials Processing Science*, vol. 27, no. 3, pp. 409–416, 1996.